Physical Characteristics of Plasma Antennas

John Phillip Rayner, Adrian Philip Whichello, *Member, IEEE*, and Andrew Desmond Cheetham, *Member, IEEE*

***Abstract*—This experimental and theoretical study examines the excitation of a plasma antenna using an argon surface wave discharge operating at 500 MHz with RF power levels up to 120 W and gas pressures between 0.03 and 0.5 mb. The results show that the length of the plasma column increases as the square root of the applied power and that the plasma density decreases linearly from the wave launcher to the end of the plasma column. These results are consistent with a simple global model of the antenna. Since noise is critical to communication systems, the noise generated by the plasma was measured from 10 to 250 MHz. Between 50 and 250 MHz the excess noise temperature was found to be 17.2 $\pm$ 1.0 dB above 290 K. This corresponds to an ohmic thermal noise source at 1.4 $\pm$ 0.3 eV, compared with an electron temperature of 1.65 eV predicted by the global model. Estimates of the electrical conductivity of the plasma column based on measured electron number densities lead to an antenna efficiency of about 65% at a transmission frequency of 100 MHz and an increase in total antenna noise of 1 dB due to the plasma. Theoretical modeling and experimental observations of the radiation pattern of the antenna show that the linear variation of conductivity and finite resistance of the column lead to a reduction in the depth of the nulls in the radiation pattern and a consequent increase in the width of the main lobe.**

***Index Terms*—Plasma antennas, plasma density, plasma electrical conductivity, plasma noise measurements, radiation efficiency, radiation patterns.**

I. Introduction

A PLASMA antenna is a radio frequency (RF) antenna using plasma elements instead of metal conductors. Such antennas are constructed from insulating tubes filled with low-pressure gases. Plasma is rapidly created and destroyed by applying bursts of RF power to the discharge tubes so the antenna can be rapidly switched on and off. When it is off, plasma is nonconducting and has no effect on the radiation pattern of other antenna elements. When it is on, plasma is an electrical conductor and, therefore, can provide the conducting medium for the radio signal.

Recent experiments have demonstrated that such antennas can be efficient and generate sufficiently low noise as to be useful for narrow band high-frequency (HF) (3–30 MHz) and very high-frequency (VHF) (30–300 MHz) communications [1], [2]. Plasma elements have a number of potential advantages over conventional metal elements for antenna design as they permit electrical, rather than mechanical control of their characteristics, including the following.

1) For military HF communications, an unenergized plasma element using single-ended excitation can be difficult to detect by hostile radar if its tube is properly designed. The antenna is only energized for a very short time as communication takes place.
2) Antenna arrays can be rapidly reconfigured without suffering perturbation from unused (i.e., switched off) plasma elements. For situations that require different antennas for several communications systems to be in close proximity (e.g., shipborne maritime communications), there is the ability to switch off antennas that are not in use. Thus, unused antennas will not couple unwanted high-power signals into nearby receivers, thus simplifying the layout of on-board communications systems.
3) With appropriate design, plasma elements can be energized and de-energized in microseconds. An antenna transmitting data at rapid rates on a low-frequency carrier could be switched at the end of each bit, thus minimizing signal degradation by antenna ringing.
4) The effective length of the antenna can be changed by controlling the applied RF power, thus allowing rapid reconfiguration of the resonant length of the antenna for different transmitting frequencies.

In addition to antennas, related areas of telecommunications where the use of plasmas have been investigated involves the production of planar plasmas for redirecting microwave signals. The frequencies used are much higher than those in this paper, as they are more geared to radar system components than to communication systems. Plasmas for possible use as microwave components include plasma sheets as reflectors for "agile" mirrors ([3]–[5]), phase shifters and plasma switches [6] which may be used in a radar system. References [7] and [8] used a hollow-cathode mechanism to produce a plasma in helium. The mechanism is similar to the aforementioned references, but the studies (so far) have been on the plasma rather than on microwave radiation properties.

References [9] and [10] produced a planar plasma by laser ionization of a gas with a low ionization potential organic impurity. The ionization mechanism is like that suggested in [3]. Experiments and theory were performed regarding both the plasma and the microwave reflection, measuring the plasma density and two-body recombination coefficient by means of microwave back-scatter plasma reflectivity and Langmuir probes.

A. Plasma Antenna Noise

Noise introduced by the plasma itself is a crucial issue when considering the use of plasma antennas for reception and transmission. Plasmas are well-known sources of noise through to microwave frequencies particularly for dc, or mains driven ac

Manuscript received May 27, 2003; revised October 20, 2003. This work was supported by University of Canberra Research Grants, an Australian Research Council (ARC) Small Grant, and the Australian Institute for Nuclear Science and Engineering (AINSE).

The authors are with the Plasma Instrumentation Laboratory, School of Information Science and Engineering, University of Canberra, Canberra ACT 2617, Australia.

Digital Object Identifier 10.1109/TPS.2004.826019

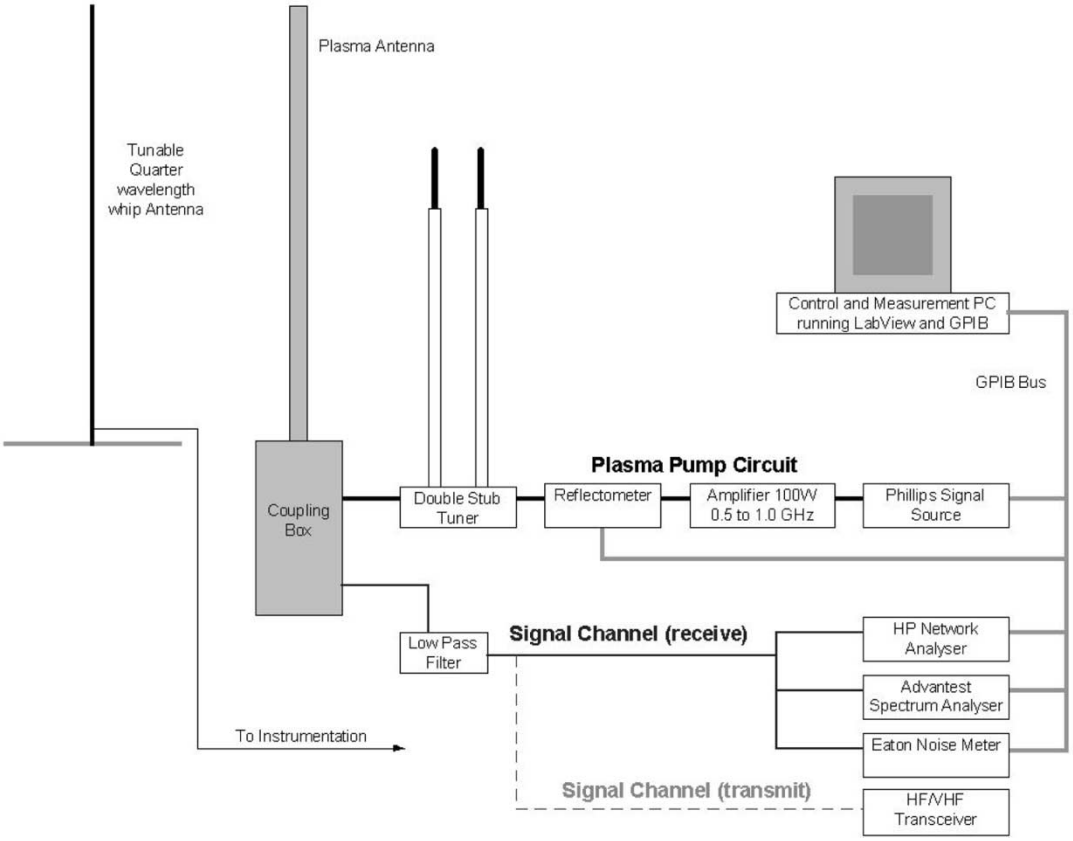

Fig. 1. Experimental arrangement. Details inside the coupling box are given in Fig. 2.

fluorescent tubes. In a communication system identification and control of the various sources of noise is of critical importance in determining the overall link budget. Early attempts to use a plasma glow discharge as an antenna were largely unsuccessful because of the amount of noise introduced by the plasma. Indeed, discharges in fluorescent tubes have been routinely used as standard noise sources up to microwave frequencies [11].

For a low-pressure glow discharge excited by a dc or low-frequency ac current a number of possible noise sources can be identified including:

1) thermal (Johnson) noise due to the random motion of the electrons characterized by the electron temperature of noise power spectral density $S_{\rm th} = 4kT_e$ WHz^{-1};
2) shot noise due to the dc current of spectral density $S_i = 2eI_{\rm DC}$ A^{2}W^{-1};
3) cathode processes including thermionic and secondary emission;
4) noise in the vicinity of the ion plasma frequency [12].

For a surface wave discharge as used in the present experiments, however, many of these processes do not occur, leaving thermal noise and the noise associated with the ion plasma frequency being the most likely contributors.

B. Paper Organization

This paper is organized as follows: Our experimental setup is described in Section II. In Section III, we determine the RF power required to excite a surface wave discharge that produces a plasma column of a specified length h (Section III-D), and to establish the form of the electrical conductivity profile along the column. We then characterize the noise generated by a plasma column excited by a surface wave (Section III-E). Results that test and confirm this theory are given in Section IV. We investigate the effects of the plasma column's conductivity profile on traditional antenna analysis in Section V and we summarize this investigation in Section VI.

II. Experimental Setup

Two different plasma antennas excited by surface waves were employed in this investigation, using the arrangement shown in Fig. 1. Antenna 1 consisted of a conventional 1.2-m fluorescent tube, filled with mercury vapor and argon at a nominal pressure of 0.4 mb. The surface wave launcher consisted of a copper "pump" collar of length 25 mm mounted 3 mm below a circular hole cut in the top of a grounded diecast box as shown in Fig. 2. RF power up to 120 W at 500 MHz was applied via a directional power meter and double stub tuner. The intense electric field developed in the gap between the collar and the box was sufficient to break down (ionize) the gas. The field then drove the resulting surface wave along the interface between the plasma and the glass tube, igniting the plasma along the column.

Experiments were undertaken for different RF power levels to determine the length of the plasma column as a function of applied RF power and the line-averaged plasma densities at heights of 15 and 36 cm above the top of the launcher using a 10 GHz microwave interferometer.

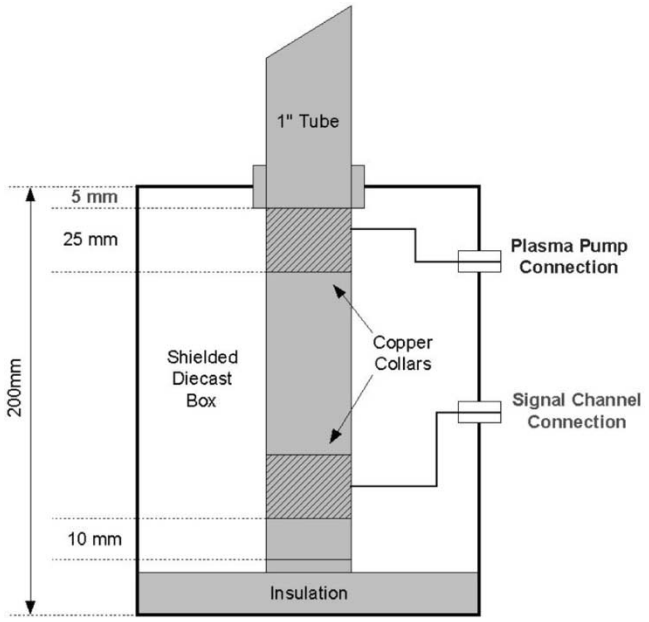

Fig. 2. Pump and transmission collar arrangement inside the coupling box of Fig. 1.

A second "transmission" (or receiving) coupling collar was mounted 10–20 mm above the tube's end cap (150 mm below the pump collar, see Fig. 2). This transmission collar was used to apply communications signals between 10 and 250 MHz to the antenna via an eight-pole low-pass filter with a corner frequency at 250 MHz when using the antenna for transmission experiments. The filter rejected the 500 MHz pump signal and also the noise associated with the +55 dB RF power amplifier used to pump the antenna. Qualitative observations have confirmed that the antenna can be used for transmitting AM or FM audio signals or TV (video) information.

Tests were also conducted using the plasma column as a receiving antenna over the range from 10 to 250 MHz for a range of RF power levels and hence different effective lengths for the antenna. Received signal strengths from a variety of laboratory and commercial sources, such as the local FM radio stations, were measured using a spectrum analyzer.

Experiments were undertaken over the range from 10 MHz to 250 MHz to determine the plasma noise (excess noise temperature) recorded at the transmission collar using an RF noise analyzer, and the antenna impedance as seen at the transmission collar using a vector network analyzer.

For comparison, an aluminum tube with the same dimensions as the fluorescent tube was used in place of the plasma antenna. For these tests the lower part of the tube was wrapped in Mylar sheet to provide an insulating layer roughly equivalent to the glass, with the two collars mounted on the tube in the same positions as for the plasma antenna. Transmission, impedance, reception, and noise measurements were repeated for the aluminum tube both with and without the pump power applied.

Antenna 2 consisted of a Pyrex glass tube with a length of 1.5 m and diameter of 20 mm connected to a vacuum pump and gas handling system that admitted argon at pressures between 0.01 and 1.0 mb to the tube in order to determine an optimum pressure for the antenna. Fig. 3 shows the simple launcher consisting

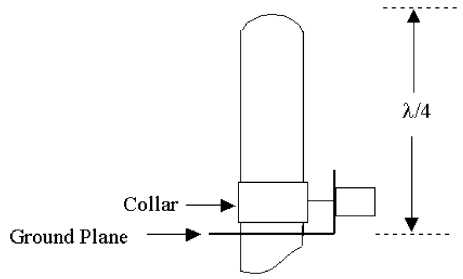

Fig. 3. Launcher pump collar arrangement for the glass antenna (Antenna 2).

of a square ground plane of side 6 cm and a collar of length 20 mm mounted 2 mm above the ground plane employed for this antenna. The launcher could be slid along the antenna to determine an optimum position for launching surface waves. This was found to be about 15 cm from the glass end cap which corresponded to a standing wave distance of $\lambda/4$ for the 500-MHz drive signal employed.

III. Theory

A. Electron Temperature

The antenna is modeled as a plasma column of radius R surrounded by an insulator of dielectric constant ϵ_g and length h determined by the RF power used to launch a surface wave at the interface between the plasma and the insulator.

A global model for a plasma source sustained by a surface wave discharge has been developed [13] and further interpreted in [14]. The electron temperature is found from a number density balance where the rate of production of electron-ion pairs by electron-neutral ionizing collisions is balanced by the radial loss of electron-ion pairs to the wall at the Bohm velocity $u_B(T_e)$, where T_e is the electron temperature and the details of the process employed to excite the plasma are not important. Thus, for unit length of the column

$$K_{\mathrm{iz}}(T_e)\, N(p) n \pi R^2 = n u_B(T_e)\, 2\pi R\, k_R(p) \tag{1}$$

where $K_{\mathrm{iz}}(T_e)$ is the rate coefficient for ionization, $N(p)$ is the neutral number density (and is a function of the filling pressure p), n is the electron density and $k_R(p)$ is a factor that relates the electron density at the edge of the sheath to its value at the center of the column. Since for the antenna $h \gg R$, losses through the end of the column can be ignored. If an explicit expression for $K_{\mathrm{iz}}(T_e)$ is substituted into (1) then it may be solved for T_e as a function of pressure and radius R. Fig. 4 shows T_e for an argon plasma over a range of pressures and radii typical of those encountered in these experiments. These values are comparable to those observed in Langmuir probe measurements in commercial fluorescent tubes of 1.6 eV for pressures between 0.1 and 0.4 mb dropping to 1.4 eV at 1.0 mb and 1.1 eV at 10 mb [15]. In particular, for $R = 1.2$ cm and $p = 100$ μb, Fig. 4 predicts an electron temperature of 1.65 eV.

B. Plasma Density

Following the analysis of [13], the plasma density is found from a power balance in which the power absorbed per unit length by the plasma from the surface wave at a position z along

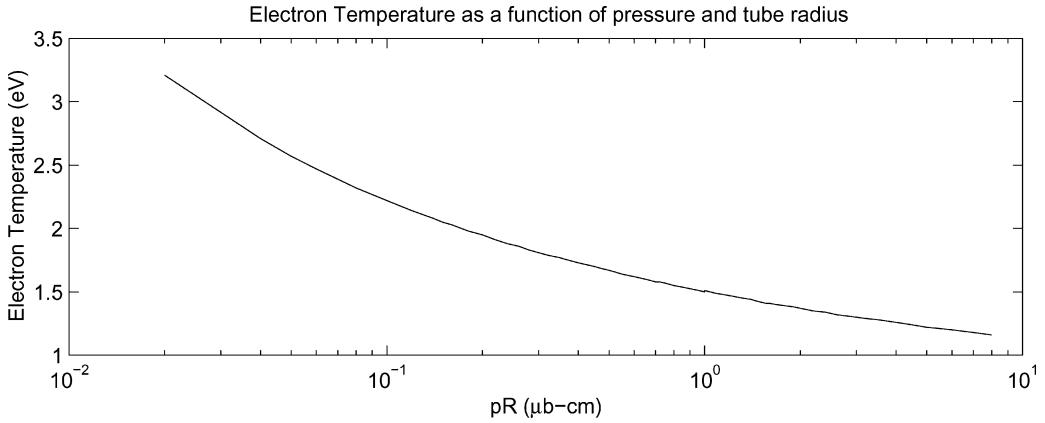

Fig. 4. Electron temperature for the plasma antenna as a function of argon pressure and tube radius, predicted by the global model.

the plasma column $A(z)$ is balanced by the power per unit length lost to the walls from the plasma $L(z)$ by the migration of electron-ion pairs at the Bohm velocity u_B. $A(z)$ is given by

$$A(z) = -\frac{dP(z)}{dz} = \alpha(z)P(z) \tag{2}$$

where $\alpha(z)$ is the attenuation coefficient and $P(z)$ is the wave power at z.

For a given tube radius R, $L(z,p)$ is given by

$$L(z,p) = u_B(T_e)\, A_{\text{eff}}(p)\, \xi_L(T_e) n(z,p) \tag{3}$$

where $A_{\text{eff}}(p) = 2\pi R k_R(p)$ is the effective surface area per unit length of the column. $\xi_L(T_e)$ is the energy loss per electron–ion pair, $n(z,p)$ is the electron number density and is a function of position and the filling pressure p. The total energy loss per electron-ion pair is made up of several contributions and is of the form ([14, p. 304])

$$\xi_L(T_e) = \xi_c + 2T_e + \xi_i \tag{4}$$

where ξ_c is the collisional loss per electron–ion pair due to ionization, excitation and elastic scattering from neutral atoms ([14, p81]). The term $2T_e$ represents the mean kinetic energy loss per electron while ξ_i is the energy loss per ion due to acceleration across the sheath ([14, p. 307]). For the conditions encountered in this investigation $\xi_L(T_e) \simeq 120$ eV.

Since u_B and ξ_L are functions of the electron temperature and hence of pressure from (1), and k_R also depends only on pressure, we may define a function

$$K(p) = u_B(p)\, A_{\text{eff}}(p)\, e\, \xi_L(p) \tag{5}$$

which is a function solely of pressure for a given geometry.

The attenuation coefficient may be determined from the dispersion relation for surface waves, with allowance being made for losses via collisions. Based on this calculation, [13] shows that $\alpha = \alpha(n)$ is essentially a function of the plasma density and suggests that a reasonable analytical approximation is of the form

$$\alpha(n) = \frac{C\nu_m}{n - n_{\text{res}}} \tag{6}$$

where C is a constant with a value $C \approx 5 \times 10^9$ m^{-4}s for these experiments and $\nu_m = \nu_m(p)$ is the electron-neutral collision frequency for momentum transfer. n_{res} is a characteristic number density at a plasma frequency corresponding to the RF frequency of the source, ω modified by the dielectric constant κ_g of the insulator (usually glass) surrounding the plasma and given by

$$n_{\text{res}} = \frac{\epsilon_0 m_e}{e^2}\, \omega^2 (1 + \kappa_g). \tag{7}$$

If the antenna is excited at the base of the column ($z = 0$) by an input power of P_0 W and the corresponding density $n_0 \gg n_{\text{res}}$, as is the case in these experiments, then combining (2) to (6) gives

$$n_0 = A(p)\sqrt{P_0} \tag{8}$$

where

$$A(p) = \sqrt{\frac{2C\nu_m(p)}{K(p)}} \tag{9}$$

and $A(p)$ is a constant for a given pressure.

C. Plasma Density Distribution Along the Antenna

The variation of density with distance along the column is found by noting that from (2) to (6)

$$P(z) = \frac{K}{2C\nu_m}\, n(n - n_{\text{res}}). \tag{10}$$

Differentiating this expression with respect to z and putting

$$\frac{dP}{dz} = -2\alpha P = -Kn \tag{11}$$

yields

$$\frac{1}{n}\frac{dn}{dz} = -\frac{2C\nu_m}{2n - n_{\text{res}}}. \tag{12}$$

At the top of the antenna $z = h$ and $n = n_{\text{res}}$, where n_{res} is the minimum value of n for which the wave propagates. Integrating (12) with this boundary condition gives at any position z

$$\frac{n(z)}{n_{\text{res}}} - \frac{1}{2}\ln\left(\frac{n(z)}{n_{\text{res}}}\right) = 1 + \frac{h - z}{L_0} \tag{13}$$

where L_0 is a characteristic length scale given by

$$L_0 = \frac{n_{\rm res}}{C\nu_m}. \tag{14}$$

In most circumstances, $n/n_{\rm res} \gg \ln(n/n_{\rm res})$, hence

$$\frac{n}{n_{\rm res}} \approx 1 + \frac{h-z}{L_0} \tag{15}$$

so that the plasma density decreases in an approximately linear fashion along the antenna. Since surface waves do not propagate for $n < n_{\rm res}$, the condition $n = n_{\rm res}$ defines the top end of the antenna. For a high-conductivity antenna with a well-defined end point, (7) shows that it is desirable to make the excitation frequency as high as possible in order to increase the value of $n_{\rm res}$.

D. Antenna Length

At the base of the antenna $z = 0$ and $n = n_0$ so that

$$h = \frac{n_0 L_0}{n_{\rm res}} - L_0. \tag{16}$$

Substituting for n_0 from (8) and recognizing that generally $h \gg L_0$, (16) may be written as

$$h \approx B(p)\sqrt{P_0} \tag{17}$$

where

$$B(p) = \sqrt{\frac{2}{CK(p)\nu_m(p)}}. \tag{18}$$

Equation (17), therefore, shows that for a given pressure the length of the antenna should increase as the square root of the applied RF power. Hence, for a given transmitting frequency it should be possible to produce the correct resonant length for, say, a quarter wave monopole by controlling the applied power. However, since the plasma density and, hence, conductivity of the antenna varies along its length the physical length of the plasma column is not necessarily the same as the electrical length of the antenna.

E. Antenna Noise

In this investigation, the frequency of the surface wave (500 MHz), and the signal frequencies (up to 250 MHz) are small compared with a typical plasma frequency $\sim$ 10 GHz. Signals within the plasma, including those due to thermal noise fluctuations, are therefore evanescent with attenuation k_i, in the absence of collisions, given by [14]

$$k_i = \frac{\omega_p}{c} \tag{19}$$

where ω_p is the plasma frequency, c is the velocity of light, and the signal frequency is large compared with the collision frequency.

The opacity of the plasma is given by

$$\tau(r) = \int_0^r k_i(s)\, ds \tag{20}$$

from which the radiation temperature may be determined from

$$T_{\rm rad} = \int_0^R T_e(r) k_i(r) e^{-\tau(r)}\, dr \tag{21}$$

where T_e is the electron temperature.

If ω_p is assumed constant with respect to radius with a value equal to the line averaged number density across the tube determined from, say, a microwave interferometer then from (19)–(21)

$$T_{\rm rad} = T_e(1 - e^{-\omega_p R/c}). \tag{22}$$

For a typical plasma density in these experiments of 10^{18} electrons m^{-3}, a plasma frequency $\omega_p \simeq 10$ GHz and tube radius $R \simeq 1.3$ cm gives an opacity $\tau \simeq 2.5$, which implies an optically dense plasma. Hence, from (22), the radiation temperature should be comparable to the electron temperature.

For a plasma sheet operating as a microwave phase shifter where $\omega^2 \gg \omega_p^2 \gg \nu_m^2$, the attenuation of the microwave passing through the plasma sheet is very small from which it may be shown that $T_{\rm rad} \ll T_e$ so that the thermal noise contribution is very small [5], [16]. Similarly, for a plasma sheet operating as a mirror with $\omega_p \simeq 1.1\omega \gg \nu_m$, very little microwave energy is absorbed by the reflector and again $T_{\rm rad} \ll T_e$ [6].

In the case of an antenna, the geometry of the rod is such that the structure is optimized to enhance radiation (and reception). This is in contrast to a mirror where the geometry is optimized to maximize reflection. Hence, it is expected that even an optically thin plasma rod, because of its geometry, should still act as a radiator with a consequent radiation temperature close to the electron temperature.

When making noise measurements the noise source impedance compared with the input impedance R_m of the noise meter needs to be considered. Thus, if the antenna has an impedance at the transmission collar of $Z_A = R_A + jX_A$ then the available noise power P_m recorded by the meter is given by

$$P_m = P_s \frac{R_m R_A}{(R_m + R_A)^2 + X_A^2} \tag{23}$$

where P_s is the noise source power. In particular for a thermal noise source and matched system where $R_m = R_A$ and $X_A = 0$, then $P_m = kT_e$ WHz^{-1}.

For a thermal noise source the effective excess noise, N_T is often expressed in decibels relative to the noise at 290 K. Thus

$$N_T = 10 \log\left(\frac{T_e}{290}\right) \text{ (in dB)}. \tag{24}$$

In absolute terms, a temperature of 290 K corresponds to an available noise power of $kT = -174$ dBm/Hz.

F. Effect of Plasma Noise on Total Antenna Noise

An antenna with a radiation resistance R_T "sees" an effective temperature due to its environment of T_r which depends on the actual temperature field around the antenna, weighted by its radiation pattern. In addition, the plasma antenna has an ohmic resistance R_A at an effective temperature assumed to be

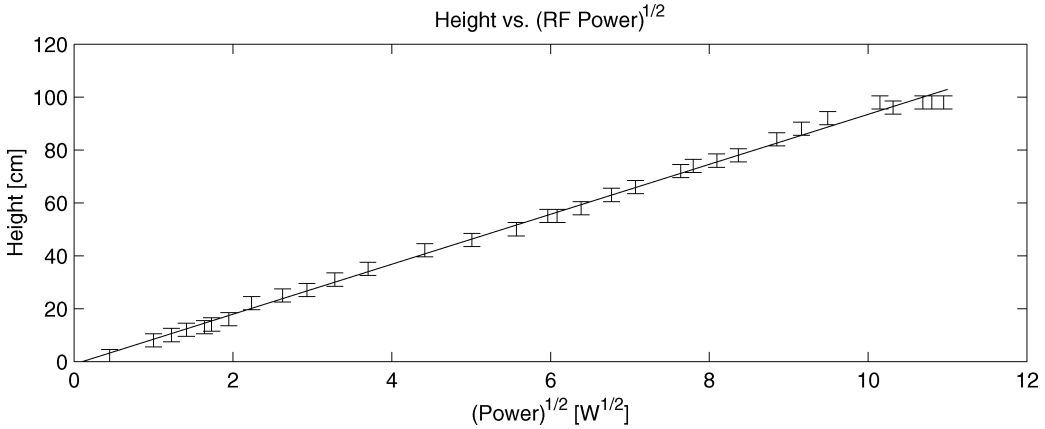

Fig. 5. Height of the plasma column as a function of $(\mathrm{RF\ Power})^{1/2}$ for the fluorescent tube.

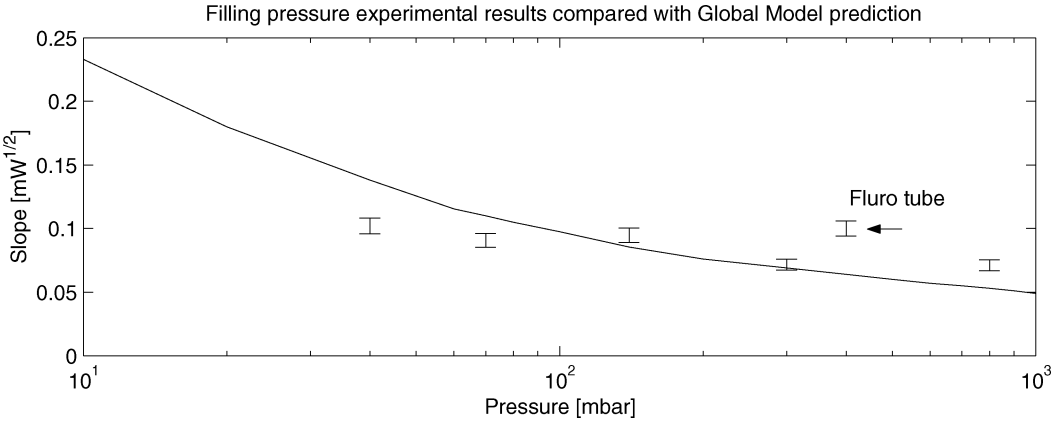

Fig. 6. $(\mathrm{Slope\ of\ Height}) \times (\mathrm{Power})^{1/2}$ plotted as a function of Pressure for Antenna 2.

the electron temperature T_e. If $R_T = R_r + R_A$ is the total resistance then the total noise temperature of the antenna T_T is given by [17]

$$T_T = T_r \frac{R_r}{R_T} + T_e \frac{R_A}{R_T}. \tag{25}$$

The efficiency of the antenna η may be defined as the ratio of the radiation resistance to the total resistance

$$\eta = \frac{R_r}{R_T}. \tag{26}$$

Thus, (25) can be written as

$$T_T = T_r \eta + T_e(1-\eta). \tag{27}$$

Equations (26) and (27) show that if $R_A \ll R_r$ so that $\eta \to 1$, then the plasma noise is minimized.

IV. Results

A. Antenna Length

The length of the plasma antenna as a function of the applied RF power was determined by observing the output of visible light from the plasma. The "end" of the antenna was assumed to be the point where the light intensity decreased quite rapidly over a distance of 5 cm. In accordance with the prediction of (17), Fig. 5 plots the height, h of the plasma column as a function of the square root of the applied power for a typical fluorescent tube of diameter 25-mm tube length above the pump collar of 1 m and a nominal filling pressure of 400 μb. The plot confirms that the length of the column increases as the square root of the applied power with a slope in this case of 9.5 ± 0.4 cm/W$^{1/2}$.

The measurements were repeated for several different fluorescent tubes and also for Antenna 2 over a range of Argon pressures between 30 and 1000 μb. In each case, the length of the column increased linearly with the square root of the power and the slope of the plot was determined. Fig. 6 plots the resulting slope as a function of pressure which is compared with the theoretical slope $B(p)$ derived from the global model in (18), assuming a value of $C = 5 \times 10^9$ m^{-4}s. The comparison shows that the results with the argon column at higher pressures agree with the global model within the error bars of the slope. The results at lower pressures are somewhat lower than predicted possibly due to some leakage of gas into the system during testing. The result for the fluorescent tube is, however, about 50% higher than predicted. This increase may be due to the presence of the easily ionized mercury vapor in the tube used for lighting purposes or the actual filling pressure being different to the assumed value of 400 μb.

B. Variation of Number Density With Column Length

Fig. 7 shows the plasma density measured at heights of 15 and 36 cm above the launcher by a 10-GHz microwave interferometer. The results have been plotted as a function of $y = h - z$,

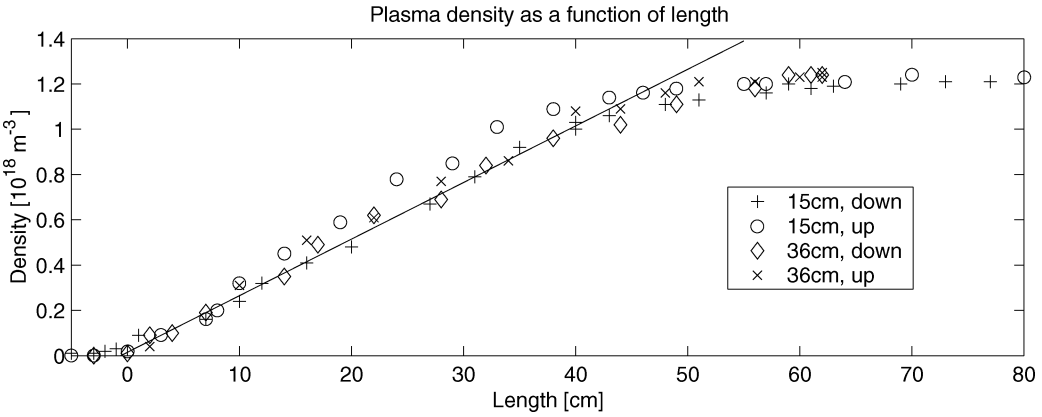

Fig. 7. Plasma density monitored at two locations as a function of the length of the column measured from the end of the column. Measurements made with increasing ("up") and decreasing ("down") power.

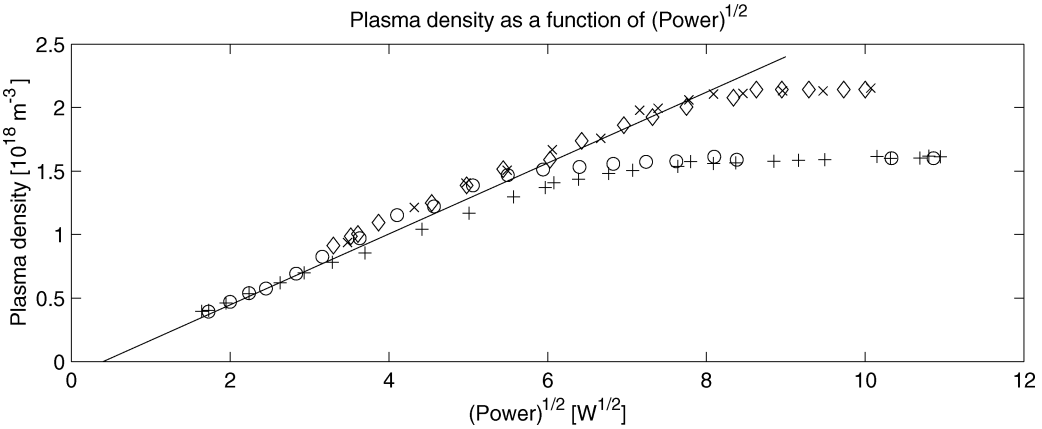

Fig. 8. Plasma density at the base of the antenna inferred from measurements at two points along the antenna as a function of $(\text{Power})^{1/2}$.

the distance measured from the top end of the column. The saturation beyond $y = 45$ cm is because the density exceeds the cut-off electron density of 1.24×10^{18} m^{-3} for a 10-GHz signal.

The results show that the density increases linearly with distance as predicted by (15) which may be rewritten in terms of y as

$$n = n_{\text{res}} + C\nu_m y. \tag{28}$$

For a typical pressure in a fluorescent tube of 400 μb, $\nu_m = 5 \times 10^8$ Hz, so that upon substituting these numerical values, (28) becomes

$$n = (0.015 + 2.5y) \times 10^{18}\ \text{m}^{-3}. \tag{29}$$

Plotting this equation in Fig. 7 shows agreement of better than 10% with the experimental data and confirms the linear variation of plasma density with length along the column.

C. Plasma Density at the Base of the Antenna as a Function of Input Power

Although it was not possible to measure the plasma density at the launcher (at the base of the antenna) it is possible to infer values by making measurements at a fixed distance z_0 from the base and using the linear variation in density established in Section IV-B. Combining (8) and (15) gives

$$n_0 = n_z - n_{\text{res}} + C\nu_m z = A(p)\sqrt{P_0}. \tag{30}$$

Measurements of n were made at $z = 15$ cm and 36 cm from which n_0 was inferred using (30) and plotted as a function of $\sqrt{P_0}$ in Fig. 8. The plot confirms that n_0 increases as the square root of the power with a slope of $A(p) = 0.28 \times 10^{18}$ m^{-3}W$^{1/2}$. For a pressure of 400 μb, the global model gives $A(p) = 0.16 \times 10^{18}$ m^{-3}W$^{1/2}$.

The results in Section IV-B confirm the theoretical value of $C\nu_m(p)$, so the discrepancy in $A(p)$ may be attributed to the experimental value of $K(p)$ being significantly less than the value predicted by the global model; that is, the loss of power to the walls by migration of electron-ion pairs is less than predicted.

D. Antenna Noise

An Eaton 2075 Noise Meter was connected to the antenna's transmission collar. Measurements were made of the excess noise generated by the plasma antenna indB above a noise temperature of 290 K (-174 dBm/Hz, or 0.025 eV) as a function of frequency. The antenna impedance was also measured over the same frequency range using a HP 7213 Network Analyzer. Fig. 9 shows the results for three different values of the RF pump power. The results have been corrected for the impedance

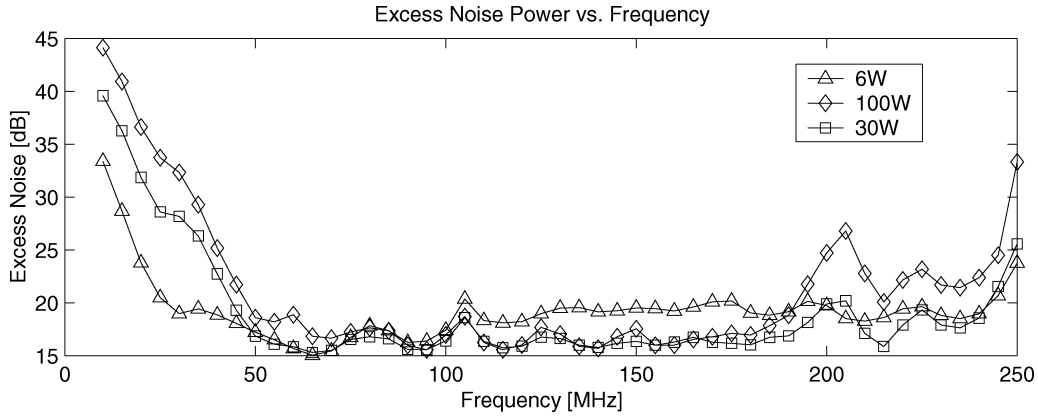

Fig. 9. Excess noise power in decibles as a function of frequency for different pump powers.

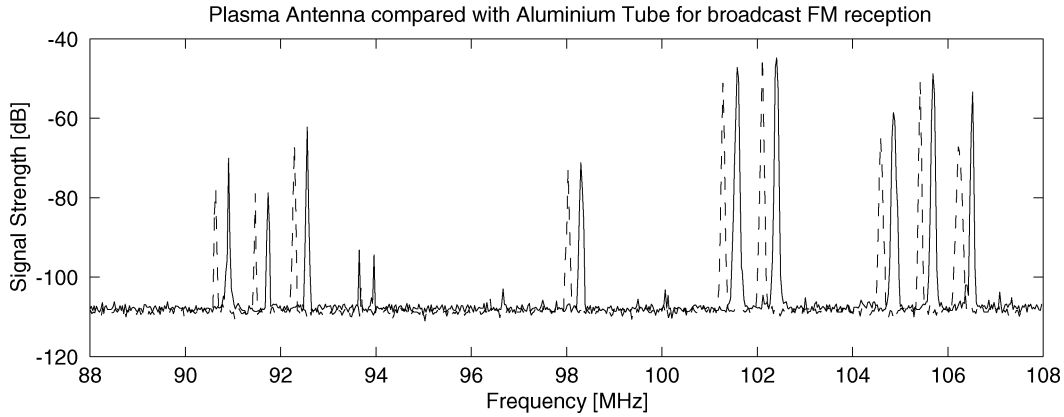

Fig. 10. Spectrum of FM radio band from 88 to 108 MHz obtained from a plasma antenna (solid) compared with an aluminum tube of the same geometry (dashed). NB: Aluminum tube antenna spectrum offset by -300 kHz for clarity.

mismatch between the antenna and the noise meter based on the impedance measurements. The plot shows that between 50 and 230 MHz the noise is essentially flat with an average equivalent excess noise of 17.2 ± 1.0 dB (1.4 ± 0.3 eV).

Fig. 4, based on the global model gives an electron temperature of 1.65 eV (18.1 dB) at 0.4 mb dropping to 1.47 eV (17.7 dB) at 1.0 mb. These results are around 17% higher than the measured noise temperatures but are sufficiently close to infer that the antenna is acting essentially as a thermal noise source operating at the electron temperature. This result is consistent with long established practice of using low-pressure discharge tubes as noise sources up to microwave frequencies. Above 230 MHz, the increase in noise is due to the noise generated by the linear power amplifier beginning to interfere with the measurements.

The increase in noise below 50 MHz is not fully understood. We suggest that it may be due to oscillations at the ion plasma frequency ω_{pi} where

$$\omega_{pi} = \omega_{pe}\sqrt{\frac{m_e}{M_i}}. \tag{31}$$

For these experiments, the plasma density ranges from 10^{17} to 2×10^{18} m^{-3} with a corresponding range of ion plasma frequencies from 3 to 50 MHz. Because of the essentially linear variation in number density along the column up to a maximum value $\sim 2 \times 10^{18}$ m^{-3} for an RF power of 100 W, a continuous range of ion plasma frequencies should exist up to a maximum around 50 MHz (as observed in Fig. 9). For an RF power of 6 W, the maximum density is 0.6×10^{18} m^{-3} with a corresponding ion frequency around 15 MHz compared with the 25 MHz observed in Fig. 9 below which the noise starts to increase.

E. Electrical Conductivity

In general the electrical conductivity of a slightly ionized plasma is given by

$$\sigma = \frac{e^2 n}{m\nu_m}. \tag{32}$$

Substituting (30) for the density and using a value of $\nu_m = 500$ MHz gives the conductivity as a function of distance in meters from the top end of the antenna

$$\sigma = 0.84 + 140y \ \mathrm{Sm}^{-1} \tag{33}$$

for values of $y \leq h$ where h is the total length of the column, and from Section IV-B, h can be related to the RF power by $h = 0.095\sqrt{P}$. Thus, for a given RF power the length of the plasma column and its conductivity profile can be determined.

F. Reception of the Broadcast FM Band

Fig. 10 shows the spectrum of the local FM band in Canberra, Australia, recorded by an Advantest 1314 spectrum analyzer. It compares the spectrum obtained using a plasma antenna 1.0 m

long with an aluminum tube of the same dimensions. The tube was mounted in the box, shown in Fig. 2, normally occupied by the plasma antenna. The tube was wrapped in a Mylar sleeve to represent the dielectric surrounding the conductor and coupled to the spectrum analyzer using the same coupling collar as the plasma antenna. Thus, apart from the conductor being either the plasma or the aluminum all other conditions should be similar in this comparison. The spectrum for the Aluminum tube has been offset by -300 kHz so that the comparison can be more clearly seen. The figure shows that the performance of the two antennas is similar in terms of the received signal strengths with the plasma antenna being typically about 4 dB higher than for the aluminum tube. This difference may be because the coupling is not quite the same due to the different dielectric materials employed and the slightly different geometry of the two configurations.

The difference in the noise floors shows that on average the noise from the plasma antenna is generally about 1.3 dB above the aluminum tube. The noise floor for the Spectrum Analyzer is about -151 dBm/Hz which translates to a noise temperature of 4.96 eV compared with the measured antenna noise temperature of 1.4 eV. The total noise temperature of 6.36 eV is equivalent to a noise signal of -149.9 dBm/Hz or an increase of 1.1 dB, which is comparable to the observed increase of 1.3 dB. The plasma antenna therefore behaves similarly to a metal conductor but at a temperature characteristic of the electron temperature of the plasma.

Within the HF/VHF band, the elevated electron temperature should not present a significant problem. A typical communications receiver for a wide-band AM signal might have an input sensitivity of 1.0 μV into 50 Ω over a bandwidth of 6 kHz for a 10 dB output signal-to-noise ratio. This is equivalent to a noise floor of -154 dBm/Hz or a noise temperature of 2.5 eV. If a plasma antenna is employed with a temperature of 1.4 eV then the noise floor of the system becomes -152 dBm/Hz so that reception is degraded by only 2 dB when a plasma antenna is employed.

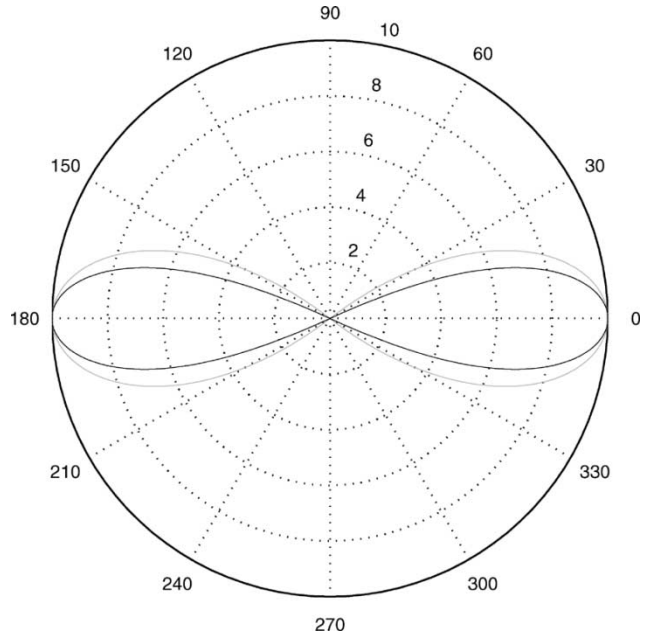

Fig. 11. Triangular varying conductivity (grey) broadens the main lobe and fills in the nulls for the $\lambda/2$ dipole antenna radiation pattern (black).

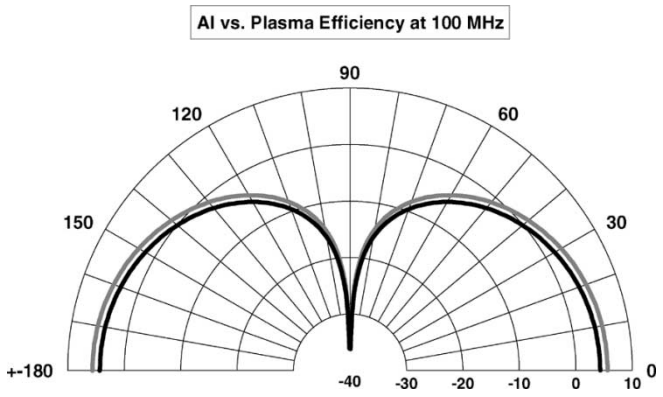

Fig. 12. Plasma (black) versus aluminum (gray) radiation efficiency. One-meter columns radiating at 100 MHz.

V. Antenna Radiation Patterns

Having now established the antenna's conductivity distribution, we will investigate its effect on the antenna's radiation pattern. The elevation radiation pattern of a simple vertical dipole of length L in free space may be found from the radiation integral [18] where the phase constant $\beta = 2\pi/\lambda$ is that of free space

$$f(\theta) = \int_{-L/2}^{L/2} I(z) e^{j\beta z \cos\theta}\, dz. \tag{34}$$

For the usual case of a good metal conductor, the current distribution $I(z)$ is usually taken to be a sinusoid over the length of the dipole

$$I(z) = I_0 \sin\left[\beta\left(\frac{L}{2} - |z|\right)\right], \qquad |z| < \frac{L}{2}. \tag{35}$$

Substituting this current distribution into (34) gives the (unnormalized) radiation pattern. The θ variation of this expression gives the far-field pattern

$$f(\theta) = \left(\frac{\cos\left[\left(\frac{L}{2}\right)\beta\cos\theta\right] - \cos\left(\frac{\beta L}{2}\right)}{\sin\theta}\right)^2. \tag{36}$$

Equation (34) may be interpreted as the Fourier transform of the current distribution to yield a far-field pattern (in terms of the Fourier variables z and the direction cosine $\beta\cos\theta$ plane wave expansion) [19], [20]

$$I(z) \overset{\text{FT}}{\Longleftrightarrow} f(\beta\cos\theta).$$

Our investigations in the previous section have led us to model the plasma antenna with a linearly decreasing conductivity distribution (Section IV-B and in [21]), which multiplies

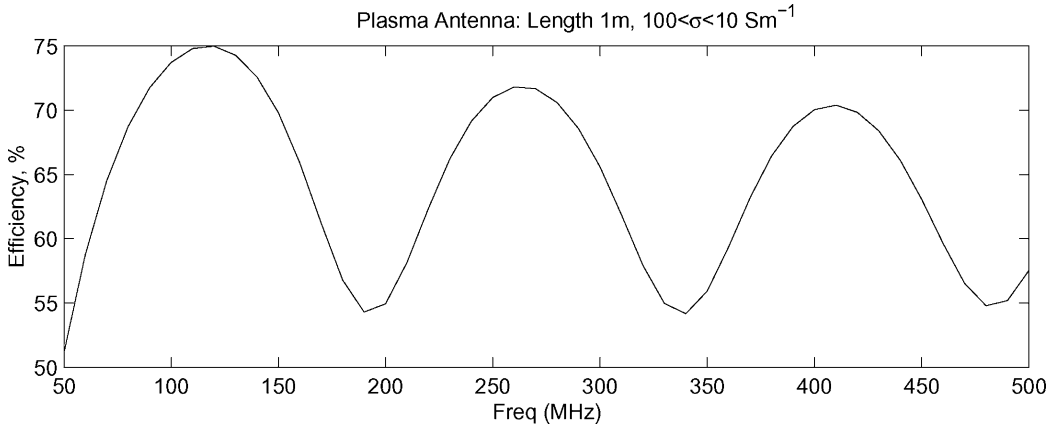

Fig. 13. Plasma antenna efficiency over the frequency band.

the usual current distribution of (35) with a triangular tapering function, $\Lambda(z)$ (also known as a triangular window). In the Fourier (far-field) domain, this convolves the far-field pattern with a sinc squared filter

$$\Lambda\left(\frac{2z}{L}\right) I(z) \overset{\mathrm{FT}}{\Longleftrightarrow} \mathrm{sinc}^2\left[\left(\frac{L}{2}\right)\beta\cos\theta\right] \otimes f(\beta\cos\theta)$$

which will broaden the far-field pattern lobes and fill in the pattern nulls (Fig. 11).

A. Computer Modeling

To numerically evaluate the integral in (34) and find the radiation pattern, we used one of the many variations of the numerical electromagnetics code (NEC) method of Moments computer packages. Several are available from http://www.qsl.net/wb6tpu/swindex.html. NEC is widely used for modeling antennas and their environment. The antenna structure is broken down into short wires and small surface areas, from which the current distribution and the radiation pattern may be found. Using a computer program, we may readily change the conductivity of the small current elements that comprise the antenna structure.

Due to the much lower conductivity of the plasma (about 100 Sm^{-1}) compared with Copper or Aluminum (more than 10^7 Sm^{-1}), plasma antennas have lower efficiencies; around 50%–60% for the equivalent length of metal [1]. Up to 75% is suggested in some of our NEC computer models, as shown in Fig. 13. RF power is lost in Joule heating of the plasma conducting elements. However, the loss is not serious, as the pattern plot in Fig. 12 shows. Here, two columns of 1 m length are radiating at 100 MHz. The Aluminum column's conductivity $\sigma = 3.5 \times 10^7$ Sm^{-1} and the plasma column has a linearly decreasing conductivity from $100 \geq \sigma \geq 10$ Sm^{-1} [21]. Only a small drop in the radiated power is observed and the shape of the radiation pattern is practically unchanged.

Over the VHF range (30–300 MHz), a plasma column plus its image of length 1 m only forms a dipole 0.1λ to about one λ in length. Therefore, the antenna is "electrically short" over most of the VHF range and the elevation angle pattern will be a slice of a torus, as shown in Fig. 14. Only at the highest frequencies is there any deviation from the usual "sideways figure-8" pattern for a half-wavelength dipole.

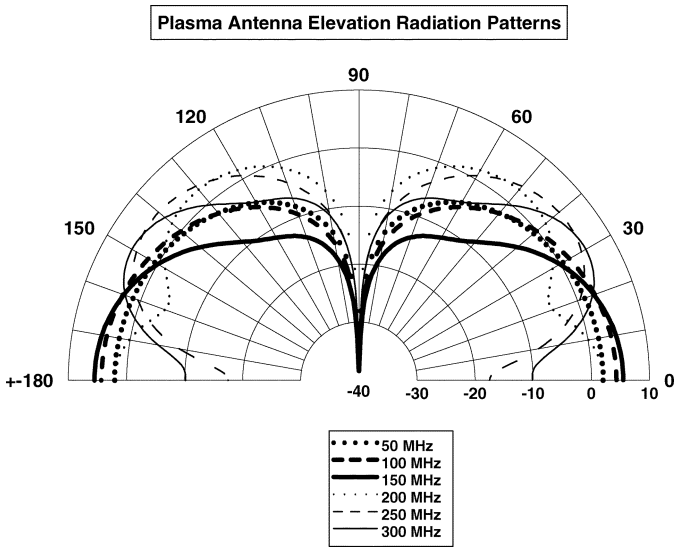

Fig. 14. Computed elevation radiation patterns for a plasma antenna with linearly varying conductivity $100 \geq \sigma \geq 10$ Sm^{-1} in the VHF range. Length of plasma column is 1 m.

Our plasma antennas are excited (or "pumped") using 500 MHz to ignite and maintain the plasma. At this frequency, the entire 1-m length of the column (plus its image) when fully lit is about 1.67λ, so the pattern structure has some distinct lobes, as shown in the upper panel of Fig. 15 (solid and dashed lines). For lower powers when only a short portion of the column length is lit, the pattern becomes more like the that of a half-wavelength dipole (dotted line).

B. Pattern Measurement

We measured the elevation patterns of our plasma antenna by moving a probe antenna in an arc over the plasma antenna under test (AUT) in 10° increments from $0° \leq \theta \leq 90°$. The probe antenna was attached to a 5.4-m rigid wooden rod, pivoted at the base where the AUT was located. Our plasma antenna is really a monopole, but this may be treated as a dipole [19] when mounted over a perfect ground plane. This produces an image of the monopole below the ground plane; when taken together with the real monopole, a dipole results. We created a suitable ground

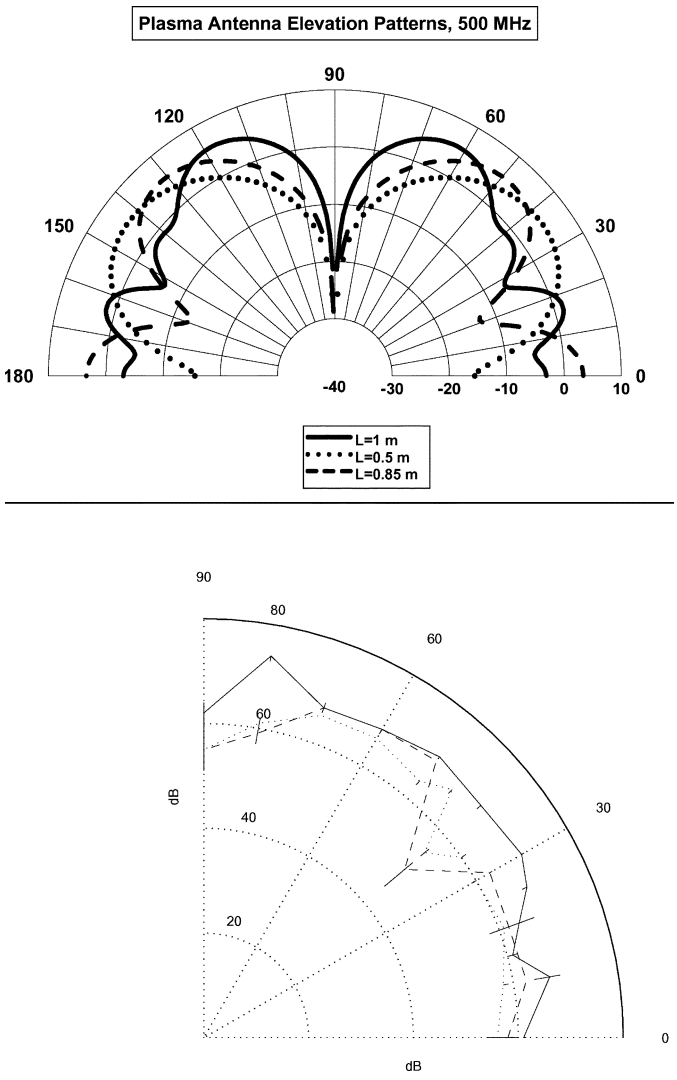

Fig. 15. (Upper) Computed elevation pattern for plasma antenna at 500-MHz pump frequency. Fully lit column length 1 m (solid), 0.85 m (dashed), and 0.5 m (dotted). (Lower) Measured elevation pattern (and associated measurement errors) for the plasma antenna at 500 MHz pump frequency.

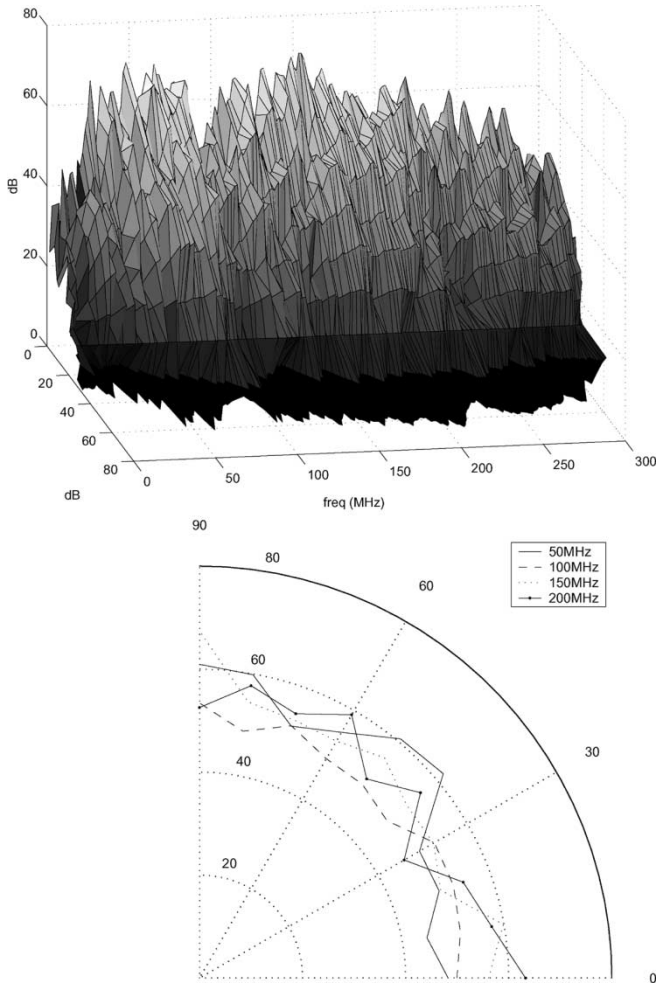

Fig. 16. (Upper) Cylindrical hidden line plot showing the measured elevation pattern for the plasma antenna over the VHF frequency band. Plasma column length: 0.85 m. (Lower) Measured elevation patterns for the plasma antenna at various VHF frequencies. These are slices of the data shown in the upper panel.

plane using the large metal mesh area of our ground reflection antenna range.

The main effect of the decreasing conductivity is to smear the pattern, broadening it and reducing the depth of the nulls. This may be seen in the measured results presented in Figs. 16 and 15 (lower panel), where the pattern has the appearance of that expected for a half-wavelength dipole (compared with Fig. 15, upper panel). It is only at the highest frequency measured and at the greatest power used that other lobe structure becomes apparent.

The measurements we were constrained to perform were really too close to the AUT at the maximum plasma column length. The Rayleigh criterion is usually taken as the minimum distance from the AUT to the far field and hence where pattern measurements should be made. It is usually taken to be greater than $2L^2/\lambda$, where L is the largest AUT dimension. For our longest effective antenna length (2 m), this is about 13 m at 500 MHz, so we are really measuring the pattern in the radiative near field, leading to filling in of the pattern nulls [22], especially the deep narrow null at zenith.

VI. Discussion And Conclusion

This investigation has established a number of the characteristics of a plasma column, when excited by a surface-wave discharge, that are necessary precursors to the use of the column as a useful antenna. It has been shown that the length of the column increases as the square root of the applied RF power and that the proportionality constant can be predicted from a simple global model within a precision of 15%. It has also been shown that the conductivity profile along the column is essentially linear. From these results it should be possible to design an antenna with an electrically controllable length, allowing rapid reconfiguration for different transmission frequencies.

If the tube becomes completely filled with plasma then the surface wave reflects from the end of the tube and deposits more energy into the top part of the tube thus leading to a more uniform distribution of conductivity along the column.

Measurements of the noise generated by the antenna confirm that above the ion plasma frequency (*ie* above 50 MHz) the plasma acts as a thermal noise source operating at the electron temperature (around 1.4 eV in this investigation). At lower frequencies the noise increases rapidly, possibly due to ion plasma oscillations.

Equation (27) indicates that the total antenna noise temperature is a function of both the antenna efficiency and the weighted temperature of the radiation field compared and the plasma noise temperature. Whether or not the plasma noise is a significant factor depends on the circumstances. For example, model calculations based on the conductivity profile established in this paper lead to an efficiency around 60% for a 0.85 m plasma antenna at 100 MHz [23]. At this frequency the sky temperature is $>$ 2000 K or 0.17 eV and so the contribution from the plasma is around 10% of the total noise temperature. Around 1 GHz, the sky temperature drops to about 20 K (0.0017 eV) which implies that a high density plasma would be required in order to maximize the efficiency and hence minimize the plasma noise component.

Unlike a conventional antenna, it is not possible to make direct electrical contact with the plasma conductor because of the insulating outer (glass) envelope or the plasma sheaths that would develop around any coupling wires inserted into the plasma. It is, therefore, necessary to use either capacitive or inductive coupling. Although capacitive coupling has been used in the present case when making the noise measurements, we have undertaken some studies to determine the most effective coupling structure [24]. However, more investigation is required to devise an efficient method for coupling the transmission signal into the antenna.

We have presented both computer modeled and measured results for the radiation pattern of our plasma antenna, at both signal and pump frequencies. These results have shown that readily available computer codes may be used to predict the radiation patterns of plasma antennas. Our investigations have shown that although there is some loss of radiation efficiency due to the lower conductivity of the plasma column, this loss is not serious and may be easily made up by slightly boosting the power used in transmission. We also found that the tapered conductivity profile has little effect on the resulting radiation pattern.

ACKNOWLEDGMENT

The authors would like to thank the reviewers for their helpful advice and comments.

REFERENCES

[1] G. G. Borg, J. H. Harris, D. G. Miljak, and N. M. Martin, "Application of plasma columns to radiofrequency antennas," *Appl. Phys. Lett.*, vol. 74, pp. 3272–3274, May 1999.

[2] G. G. Borg, J. H. Harris, N. M. Martin, D. Thorncraft, R. Milliken, D. G. Miljak, B. Kwan, T. Ng, and J. Kircher, "Plasmas as antennas: Theory, experiment and applications," *Phys. Plasmas*, vol. 7, pp. 2198–2202, July 2000.

[3] W. M. Manheimer, "Plasma reflectors for electron beam steering in radar systems," *IEEE Trans. Plasma Sci.*, vol. 19, pp. 1228–1234, Dec. 1991.

[4] A. E. Robson, R. Morgan, and R. Meger, "Demonstration of a plasma mirror for microwaves," *IEEE Trans. Plasma Sci.*, vol. 20, pp. 1036–1040, Dec. 1992.

[5] R. F. Fernsler, W. M. Manheimer, R. A. Meger, J. Mathew, D. P. Murphy, R. E. Pechacek, and J. A. Gregor, "Production of large area plasmas by electron beams," *Phys. Plasmas*, vol. 5, pp. 2137–2144, 1998.

[6] W. M. Manheimer, R. F. Fernsler, and M. S. Gitlin, "High power, fast, microwave components based on beam generated plasmas," *IEEE Trans. Plasma Sci.*, vol. 26, pp. 1543–1555, Oct. 1998.

[7] S. Larigaldie and L. Caillault, "Dynamics of a helium plasma sheet created by a hollow cathode electron beam," *J. Phys. D, Appl. Phys.*, vol. 33, pp. 3190–3197, 2000.

[8] L. Caillault and S. Larigaldie, "Mechanisms of a linear hollow cathode used for the production of a helium plasma sheet," *J. Phys. D, Appl. Phys.*, vol. 35, pp. 1010–1019, 2002.

[9] W. Shen, J. E. Scharer, N. T. Lam, B. G. Porter, and K. L. Kelly, "Properties of a vacuum ultraviolet laser created plasma sheet for a microwave reflector," *J. Appl. Phys.*, vol. 78, no. 12, pp. 6974–6979, 1995.

[10] K. L. Kelly, J. E. Scharer, G. Ding, M. Bettenhausen, and S. P. Kuo, "Microwave reflections from a vacuum ultraviolet laser produced plasma sheet," *J. Appl. Phys.*, vol. 85, no. 1, pp. 63–68, 1999.

[11] T. S. Laverghetta, *Handbook of Microwave Testing*. Norwood, MA: Artech House, 1981, p. 144.

[12] L. J. Spitzer, *Physics of Fully Ionised Gases*. New York: Interscience, 1957, p. 63.

[13] M. Moisan and Z. J. Zakrzewski, "Plasma sources based on the propagation of electromagnetic surface waves," *J Phys D, Appl. Phys.*, vol. 24, pp. 1025–1048, 1991.

[14] M. A. Lieberman and A. J. Lichtenberg, *Principles of Plasma Discharges and Materials Processing*. New York: Wiley, 1994, pp. 443–447.

[15] J. F. Weymouth, *Plasma Diagnostics in Electric Discharge Light Sources*. San Diego, CA: Academic, 1989, vol. 1, p. 65.

[16] D. P. Murphy, R. F. Fernsler, R. E. Pechacek, and R. A. Meger, "Microwave emission from plasmas produced by magnetically confined electron beams," *IEEE Trans. Plasma Sci.*, vol. 30, pp. 436–441, Feb. 2002.

[17] E. C. Jordan and K. G. Balmain, *Electromagnetic Waves and Radiating Systems*, 2nd ed. Englewood Cliffs, NJ: Prentice-Hall, 1965, pp. 414–416.

[18] W. L. Stutzman and G. A. Thiele, *Antenna Theory and Design*, 2nd ed. New York: Wiley, 1998, pp. 164–173.

[19] C. A. Balanis, *Antenna Theory*. New York: Wiley, 1997, pp. 165–173.

[20] E. O. Brigham, *The Fast Fourier Transform and its Applications*. Englewood Cliffs, NJ: Prentice-Hall, 1988, pp. 349–357.

[21] J. P. Rayner, A. P. Whichello, and A. D. Cheetham, "Physical characteristics of a plasma antenna," in *Proc. 11th Int. Conf. Plasma Physics*, Sydney, Australia, July 2002, pp. 392–395.

[22] G. E. Evans, *Antenna Measurement Techniques*. Norwood, MA: Artech House, 1990.

[23] A. P. Whichello, J. P. Rayner, and A. D. Cheetham, "Plasma antenna radiation patterns," in *Proc. 11th Int. Conf. Plasma Physics*, Sydney, Australia, July 2002, pp. 396–399.

[24] M. Hargreave, J. P. Rayner, A. D. Cheetham, G. N. French, and A. P. Whichello, "Coupling power and information to a plasma antenna," in *Proc. 11th Int. Conf. Plasma Physics*, Sydney, Australia, July 2002, pp. 388–391.

John Phillip Rayner received the Ph.D degree in physics in the field of hypervelocity aerodynamics from the Australian National University, Canberra, in 1974.

Since then, he has combined his research work with a career in higher education in physics and engineering principally at the University of Canberra, Canberra. He is currently the Head of the School of Information Sciences and Engineering, University of Canberra. His research interests include plasma engineering with particular interests in plasma antennas, helicon plasma sources, instrumentation and control systems, and also educational innovation in engineering.

Adrian Philip Whichello (M'99) was born in Sydney, Australia. He received the B.Sc. degree (with honors) in physics from the the University of New South Wales (NSW), Sydney, the M.Sc. degree (with honors) in geophysics from Macquarie University, NSW, Australia, and the Ph.D degree in electrical engineering from the University of NSW.

He joined the Division of Radiophysics, CSIRO, Sydney, where he worked on designing microwave antennas for the INTERSCAN project. He then moved to the CSIRO Division of Atmospheric Research (Cloud Physics Laboratory), to assist the research on storm formation over the Southern Ocean. With the closure of the Cloud Physics Laboratory, he held tutoring and lecturing positions at the University of NSW and then the University of Western Sydney, Sydney, in physics and engineering. He has worked on pattern recognition problems with the Department of Electrical Engineering, Sydney University, and with the Australian Defence Force Academy. He is currently lecturing on digital signal processing (DSP) with the School of Information Science and Engineering, University of Canberra, Canberra, Australia, where he is also the IEEE Student Branch Councellor. His research interests include signal and image processing, antenna measurements, and pattern recognition.

Andrew Desmond Cheetham (M'99) received the Ph.D. degree in plasma physics from Flinders University, Adelaide, South Australia.

After receiving the degree he spent 15 years working in the field of plasma measurement systems in national fusion research laboratories in the University of Stuttgart, Stuttgart, Germany; Ecole Polytechnique Federale de Lausanne, Lausanne, Switzerland; Australian National University, Canberra, Australia. He then became a Principal Scientist at the JET Joint Undertaking, Culham, U.K. In 1990, he joined the Australian Tertiary Education System in the School of Electronics and Telecommunications Engineering, University of Canberra, Canberra, where he has lectured in physics, electronics, instrumentation, and automatic control systems, as well as directing the Plasma Instrumentation Laboratory. He is currently Pro Vice-Chancellor of Research and Information Management.